Interdisciplinary Studies on Applied Science, 3(1):66–75, 2026. DOI: 10.58613/isas316

Interdisciplinary Studies on Applied Science

Journal homepage: https://gpub.org/journal-details.php?journal-id=42

ISSN (E): 3048-877X

Research Article

Hydrogeological Controls on Groundwater Contamination from Petroleum Operations: Contaminant Migration, Aquifer Vulnerability, and Assessment Methods

Bernard Nkrumah Attobrah [1*], Emmanuel Kobina Gyasi [2], Elijah Asamoah Amoateng [3], Enoch Nii-Okai [4], Mariam Iyabo Adeoba [5], Jonathan Kuffour Owusu [6] and Aderemi Sarah Aduloju [7]

[1]*Department of Earth and Environmental Sciences, New Mexico Institute of Mining and Technology, Socorro, New Mexico, USA.*
[2]*Department of Geology, Kansas State University, Manhattan, Kansas, USA.*
[3]*Department of Physical Sciences, Eastern New Mexico University, Portales, New Mexico, USA.*
[4]*Department of Geological and Mining Engineering and Sciences, Michigan Technology University.*
[5]*Department of Mechanical, Bioresources and Biomedical Engineering, University of South Africa, Florida, Johannesburg, South Africa.*
[6]*Fort Hays State University, Department of Geosciences, Hays, Kansas USA.*
[7]*Department of Geophysics, Federal University Oye-Ekiti, Oye-Ekiti, Nigeria.*
[*]*Corresponding author: bernard.attobrah@yahoo.com*

Article Info

Keywords: *Groundwater contamination, Petroleum hydrocarbons, LNAPL, Aquifer vulnerability, DRASTIC, Contaminant migration, Natural source zone depletion, Hydrogeology.*

Received: *01.04.2026;*
Accepted: *11.04.2026;*
Published: *15.04.2026*

© 2026 by the author's. The terms and conditions of the Creative Commons Attribution (CC BY) license apply to this open access article.

Abstract

Petroleum hydrocarbons enter groundwater from every stage of the oil and gas supply chain, drilling, pipeline transport, refining, storage, and retail distribution, and persist in aquifer systems as free-phase, dissolved, residual, and vapor-phase contaminants for decades after the initial release. How severely a given release affects groundwater depends less on spill volume or operation type than on the hydrogeological properties of the receiving aquifer. This narrative review evaluates the controls that govern that relationship, drawing on field evidence published between 2010 and 2025 from Scopus, Web of Science, and Google Scholar. Four domains are addressed: contaminant migration and fate, including multiphase flow behavior and natural source zone depletion rates measured across 40 petroleum sites at a median of 9,540 L/ha/yr; aquifer vulnerability assessment, comparing DRASTIC, GOD, and physically-based transport models across alluvial, karst, and fractured settings; hydrogeological controls on contamination severity, with depth to the water table, lithology, fracture connectivity, and water table fluctuation identified as the dominant factors; and field assessment and monitoring methods, from standard hydrochemical indicators through compound-specific isotope analysis and geophysical imaging. Index-based vulnerability frameworks provide useful regional screening but produce vulnerability estimates differing by a factor of four when multiple models are applied to identical input data, and none account for the temporal evolution driven by biodegradation. Site characterization that pairs index screening with multi-parameter field investigation, hydrochemistry, redox profiling, isotopic analysis, and geophysical spatial coverage, would bring routine practice closer to the level of understanding that the available science already supports.

How To Cite: B.N. Attobrah, E.K. Gyasi, E.A. Amoateng, E. Nii-Okai, M.I. Adeoba, J.K. Owusu, A.S. Aduloju. Hydrogeological Controls on Groundwater Contamination from Petroleum Operations: Contaminant Migration, Aquifer Vulnerability, and Assessment Methods. *Interdisciplinary Studies on Applied Science*, 3(1):66–75, 2026. https://doi.org/10.58613/isas316

1. Introduction

Groundwater supplies drinking water to over two billion people and sustains irrigated agriculture across every continent, even as its quality declines in both urban and rural settings worldwide [1, 2]. Among the anthropogenic threats to aquifer systems, petroleum hydrocarbons occupy a particular position: they enter the subsurface from nearly every stage of the oil and gas supply chain, wellsite drilling and production, pipeline transport, refinery processing, tank farm storage, and retail fuel distribution, and once below ground, they persist for decades as free-phase, dissolved, residual, and vapor-phase contaminants [3]. Underground fuel storage tanks alone, with typical service lives of 15–25 years, leak at rates as low as two drops per second, yet can render hundreds of millions of liters of groundwater unfit for consumption [4]. The BTEX compounds (benzene, toluene, ethylbenzene, xylenes) and polycyclic aromatic hydrocarbons that partition from petroleum into groundwater are classified as priority pollutants by both the WHO and the US EPA based on their mutagenic, carcinogenic, and endocrine-disrupting properties [3, 5].

What makes petroleum contamination of groundwater especially difficult to manage is that the subsurface behavior of these compounds is governed not by the spill itself but by the aquifer receiving it. The same volume of crude oil released into a shallow sandy alluvial aquifer with a water table at two metres will produce a fundamentally different contamination pattern than the same release into a deep fractured karst system where conduit flow reaches thousands of meters per day. Depth to the water table, lithology, hydraulic conductivity, fracture density, recharge regime, and the geochemical environment controlling biodegradation all mediate the transition from surface release to aquifer contamination, and they do so in combinations that vary from site to site [6, 7]. Vulnerability assessment frameworks such as the DRASTIC index attempt to capture this complexity through weighted parameter overlays, but their reliance on subjective scoring has drawn persistent criticism, and physically-based transport models that avoid this subjectivity remain computationally expensive at regional scales [8].

Several reviews have addressed parts of this problem individually. Mineo (2023) cataloged the LNAPL contamination literature from 2012 to 2022 and organized it by laboratory, field, and modeling approaches but without comparing how aquifer properties control contamination outcomes across different petroleum operation types [6]. Kulkarni et al. (2022) compiled NSZD rates from 40 sites but focused on attenuation measurement rather than the hydrogeological factors governing why rates differ between sites [9]. Kuppusamy et al. (2020) reviewed petroleum hydrocarbon fate and remediation broadly but did not synthesize the vulnerability assessment or geophysical characterization literature [3]. No recent work has drawn these threads together, migration mechanics, vulnerability mapping, hydrogeological controls, and field assessment methods, into a single review framed around the question of what makes one aquifer more at risk than another when petroleum enters the subsurface.

This review takes that approach. The objective is to evaluate how hydrogeological properties control the severity of groundwater contamination from petroleum operations spanning the full supply chain and to compare the assessment frameworks used to characterize that risk. The scope covers onshore aquifer systems at depths of 0–150 m, drawing primarily on field evidence from 2010 to 2025, with foundational sources retained where no recent alternatives exist. A companion paper evaluates the geophysical methods used to detect and delineate hydrocarbon contamination in the subsurface; the present review addresses the contamination system itself, how petroleum moves, what makes aquifers vulnerable, and how that vulnerability is measured.

Figure 1 illustrates the four coexisting contamination phases and the redox zonation that governs biodegradation in the subsurface.

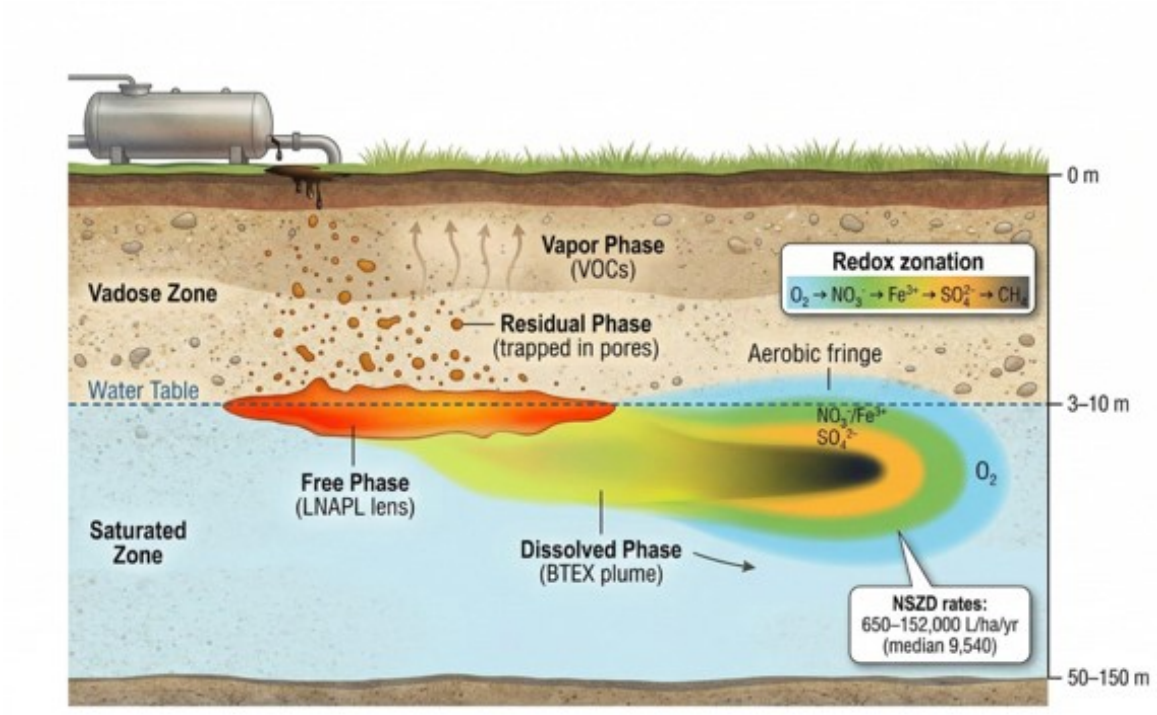

Figure 1: LNAPL fate and migration in the subsurface following a petroleum release

2. Methods

Published literature on hydrogeological aspects of groundwater contamination from petroleum operations was gathered from Scopus, Web of Science, and Google Scholar over January–March 2026. The search targeted six broad concept areas, LNAPL migration and multiphase flow, aquifer vulnerability indexing, natural source zone depletion, vadose zone transport, hydrochemical and isotopic biodegradation indicators, and geophysical site characterization, without imposing Boolean strings or fixed keyword combinations. This is a narrative review; no systematic protocol, PRISMA checklist, or meta-analytic pooling was applied.

Studies qualified for inclusion if they reported quantitative subsurface data from petroleum-contaminated sites: measured contaminant concentrations, hydraulic parameters, vulnerability scores, depletion rates, or isotopic fractionation values from field campaigns or field-validated models. Pure remediation performance evaluations, marine settings, DNAPL-only studies, and health risk assessments that lacked subsurface transport data were set aside, as were non-English texts and conference abstracts without accessible full papers. Most of the evidence dates from 2010 onward, though a handful of older sources, the 1987 DRASTIC framework, foundational capillary pressure relationships, and the Bemidji long-term monitoring record, were kept because nothing published since has replaced them.

Two recent review articles served as starting points for reference-list snowballing: Mineo (2023) for the broader LNAPL contamination literature and Kulkarni et al. (2022) for NSZD field measurements. Chasing citations through those reference lists continued until no new qualifying studies appeared. From each included study, seven descriptors were recorded: aquifer type, contamination source and petroleum operation, contaminant identity, depth investigated, hydrogeological measurements taken, assessment approach, and headline quantitative result. The collected evidence was then sorted into four thematic groups and evaluated narratively, weighing consistency of findings across sites, spread of geographic coverage, and soundness of field methods, but without scoring individual studies on a formal risk-of-bias scale.

3. Results

3.1. Contaminant Migration and Fate

Petroleum hydrocarbons released at the surface migrate downward through the vadose zone as a three-phase system governed by gravity, capillary pressure, and relative permeability. Zou et al. (2021) tracked diesel infiltration through layered sand-tank experiments in China and found that vertical migration velocity in medium and coarse sand exceeded that in fine sand by one order of magnitude [10]. Diesel accumulated at coarse-to-fine interfaces where capillary entry pressure created a barrier and reached equilibrium retention within 96 hours of release. Precipitation displaced 40.78% of free-phase LNAPL in coarse sand but only 10% in fine sand, confirming that grain size controls both initial migration and rainfall-driven redistribution [10]. Han et al. (2025) extended this work to the capillary zone specifically, using diesel in fine sand and silty sand columns at the Zhangjiawan experimental site in Beijing. LNAPL stopped flowing within 20–40 cm of the water table in fine sand and within 30–50 cm in silty sand, the difference attributable to higher moisture content reducing NAPL-phase relative permeability [11]. Suo et al. (2025) monitored LNAPL migration in heterogeneous sandy media using cross-hole electrical resistivity tomography in Henan, China, and recorded average vertical migration rates of 1.06 cm/h under unsaturated conditions, 0.51 cm/h at a constant water table, and 1.45 cm/h when the water table declined, demonstrating that falling water levels accelerate LNAPL advance by reducing capillary resistance [12].

Upon reaching the water table, LNAPL spreads horizontally to form a floating lens whose geometry depends on release volume, fluid viscosity, and hydraulic gradient. Mineo and Ferrara (2022) tracked the evolution of a hydrocarbon plume in a fractured limestone aquifer in southeastern Sicily over six years (2014–2020) and found that apparent LNAPL thickness in monitoring wells correlated with groundwater oscillation amplitude [13]. Seasonal water table fluctuations redistributed free-phase product vertically across the smear zone, rising levels trapped LNAPL as residual, while falling levels remobilized it. The plume migrated along fracture orientations that deviated from the regional groundwater flow direction, indicating that geological structure rather than hydraulic gradient controlled migration in this fractured setting [13].

Table 1 summarizes the design, setting, and headline findings of the studies examined across all four thematic domains.

Biodegradation progressively depletes LNAPL mass through sequential consumption of electron acceptors. The Bemidji crude oil research site in Minnesota, monitored continuously since a 1979 pipeline rupture that released approximately 10,700 m³ of crude oil, provides the longest field record of this process. Essaid et al. (2011) documented 25 years of geochemical evolution across the plume [14]. Reactive transport modeling by Ng et al. (2015) attributed over 80% of observed carbon efflux at Bemidji to direct-contact biodegradation and outgassing of methane and carbon dioxide, rather than aqueous-phase dissolution [15]. Kulkarni et al. (2022) compiled natural source zone depletion (NSZD) rates from 40 petroleum LNAPL sites across the United States and reported a median site-average rate of 9,540 L/ha/yr (range: 650–152,000 L/ha/yr), with no statistically measurable difference between fuel types [9]. Rates varied seasonally, with a median Q10 value of 2.11, indicating that a 10°C temperature increase could approximately double the depletion rate [9]. Mackay et al. (2024) separated three NSZD mechanisms at a California site containing both aliphatic-rich naphtha and aromatic-rich pyrolysis gasoline within the same geological setting: methanogenesis dominated in the aliphatic zone at 10,000 mg C/m²/d and vaporization dominated in the aromatic zone at 400 mg C/m²/d, while aqueous biodegradation contributed 67–92 mg C/m²/d in both zones [16]. The governing attenuation pathway at a given source zone is determined by the LNAPL chemical composition, rather than solely by geological factors, according to these findings.

Table 1: Characteristics of key studies reviewed

Ref	Study	Operation / Source	Site / Country	Aquifer	Depth	Method	Key Finding	Notable Limits
[10]	Zou et al. (2021)	Diesel spill (lab)	China	Layered sand (lab)	0–1 m	Sand-tank experiment	Migration in coarse sand 10× faster than fine; rainfall displaced 40.78% vs 10%	Lab scale only
[11]	Han et al. (2025)	Diesel (lab)	Beijing, China	Fine sand / silty sand	Capillary zone	Sand-tank + TMVOC modeling	LNAPL stopped 20–40 cm above water table in fine sand, 30–50 cm in silty sand	Single contaminant
[12]	Suo et al. (2025)	LNAPL (lab)	Henan, China	Hetero-geneous sand	0–0.5 m	Cross-hole ERT	Migration rates: 1.06 cm/h unsaturated, 0.51 cm/h constant WT, 1.45 cm/h declining WT	Lab tank, not field
[13]	Mineo & Ferrara (2022)	Tank leak	Sicily, Italy	Fractured limestone	0–30 m	6-year plume monitoring	LNAPL thickness correlated with WT oscillation; fracture-controlled migration	Single site
[14]	Essaid et al. (2011)	Pipeline rupture (1,700 m³)	Bemidji MN, USA	Glacial outwash sand	0–12 m	25-year geochemical monitoring	Plume evolution from aerobic to methanogenic conditions over decades	Single crude oil type
[15]	Ng et al. (2015)	Same Bemidji spill	Bemidji MN, USA	Glacial outwash sand	0–12 m	Reactive transport model	>80% carbon efflux from direct outgassing, not aqueous dissolution	Model-dependent
[9]	Kulkarni et al. (2022)	Multiple fuel types	40 sites, USA	Various	Various	NSZD rate compilation	Median 9,540 L/ha/yr (range 650–152,000); Q10 = 2.2; no fuel-type difference	Measure-ment method variability
[16]	Mackay et al. (2024)	Naphtha + pyrolysis gasoline	California, USA	Same geology, dual source	Vadose + saturated	Three-mechanism NSZD	Methanogenesis 1,000 mg C/m²/d (aliphatic); vaporization 400 (aromatic)	Single site, two zones
[17]	Jha et al. (2019)	Agricultural + industrial	Chhattisgarh, India	Alluvial	Variable	GIS-DRASTIC	17.34% very high, 23.72% high; 82.35% validation accuracy vs nitrate	Nitrate proxy, not petroleum
[18]	Zarei et al. (2022)	Agricultural	Fasarood, Iran	Alluvial plain	Variable	DRASTIC + 3 variants	All 4 models: low–moderate; composite DRASTIC best spatial correlation	No petroleum -specific validation
[19]	Chitsazan & Akhtari (2009)	Petroleum region	Khuzestan, Iran	Alluvial	Variable	GIS-DRASTIC	Shallow WT + permeable sand + petroleum proximity = highest scores	No contaminant validation
[20]	Jalali & Kolahchi (2019)	Mixed	Hamadan, Iran	Alluvial	Variable	DRASTIC, GOD, SI, SINTACS	High-vulnerability area: 7.1% (DRASTIC) to 44.21% (SI) — fourfold range	Same data, divergent outputs
[21]	Umar et al. (2024)	Pipeline oil spills	Ahoada, Niger Delta	Benin Fm sand	<5 m WT	Modified DRASTIC + pipeline	Pipeline-adjusted index outperformed standard; ROC/AUC validated vs PAH	Single region

Table 1 Continuous

Ref	Study	Operation / Source	Site / Country	Aquifer	Depth	Method	Key Finding	Notable Limits
[22]	Muneer et al. (2025)	Petroleum exploration	Karak, Pakistan	Fold-thrust belt	Variable	GIS-DRASTIC	Fractured zones >150 index (high); confined aquifers <100	No field contamination data
[23]	Soriano et al. (2022)	Un conventional O&G spills	Appalachian Basin, USA	Surficial aquifer	0–150 m	MODFLOW-6 + ML metamodels	250 m resolution; <10 yr travel time = high risk; ML failed across domains	Steady-state assumption
[24]	Zanello et al. (2021)	Residual fuel (modeled)	Bahía Blanca, Argentina	3 textures modeled	1.5–8 m WT	HYDRUS-1D transport sim.	Sandy loam very high risk to 8 m; silt/clay moderate beyond 5 m	Steady WT; no NAPL phase
[25]	Karimova et al. (2021)	Petrochemical refinery	Pavlodar, Kazakhstan	Alluvial, T = 22–133 m²/d	2–51 m	MODFLOW + MT3DMS	TPH plumes km-scale; all wells exceeded permissible limit	Limited monitoring data
[26]	Abo-Tabikh et al. (2025)	Power station HFO leak	Northern Jordan	Karst limestone	∼50 m	Pump-and-treat + CSM	GW velocity 218–9,500 m/d; TPH >10 → <0.5 mg/L after remediation	Single karst site
[27]	Ruggieri et al. (2017)	Drilling fluid loss	Sicily, Italy	Karstified carbonate	Epikarst	Spring monitoring	Recharge velocity 230 m/h; spring contaminated for weeks	Accidental, not petroleum product
[28]	Guo et al. (2021)	Petroleum since 1980s	Zibo, Shandong, China	Fractured karst	0–50 m	TMVOC + hydro chemistry	Large-amplitude concentration oscillations; requires continuous monitoring	Complex multi-source history
[29]	Cozzarelli et al. (2022)	Same Bemidji spill	Bemidji MN, USA	Glacial outwash sand	0–12 m	40-year hydro-chemistry	Redox zonation $O_2 \rightarrow NO_3^- \rightarrow Fe^{3+} \rightarrow SO_4^{2-} \rightarrow CH_4$; benzene down >90%	Single site
[30]	Babika et al. (2024)	Oil spills (multiple)	Niger Delta, Nigeria	Benin Fm sand	<10 m	Sub-catchment sampling	GW TPH 3–473 mg/L; PAH up to 0.28 mg/L; 54–100% exceedance	15 stations only
[31]	Mancini et al. (2002)	Industrial contamination	Netherlands	Alluvial	Shallow	Dual CSIA (δ^{13}C)	δ^{13} C + 2‰, δ^2H +27–50‰ = anaerobic biodegradation confirmed	Single plume
[32]	Sherwood Lollar et al. (2022)	Chemical manufacturing	New Jersey, USA	Alluvial	Shallow	Dual CSIA + Rayleigh eq.	47–99% DCB degradation; 21–73% TCB degradation quantified	Mixed chlorobenzene-BTEX
[33]	Li et al. (2024)	Industrial contamination	Shandong, China	Alluvial	Shallow	CSIA + 5-year monitoring	δ^{13}C enrichment +2.9 to +27.3 ‰; sulfate-reducing bacteria dominant	Pesticide site, not petroleum
[34]	Dong et al. (2024)	Chemical plant	Eastern China	Silt/fine sand	Shallow	Time-domain IP imaging	α <5 mS/m = contaminated; phase <20 mrad = source zone vs plume	Single profile

3.2. Aquifer Vulnerability Assessment

The DRASTIC index, a weighted overlay of seven hydrogeological parameters (depth to water table, net recharge, aquifer media, soil media, topography, impact of vadose zone, and hydraulic conductivity), remains the most widely applied framework for mapping groundwater vulnerability in petroleum-affected regions. In the Tandula watershed of Chhattisgarh, India, Jha et al. (2019) applied GIS-based DRASTIC and classified 17.34% of the area as very high vulnerability, 23.72% as high, and 18.68% as very low [17]. Validation against nitrate concentrations in 34 monitoring wells yielded 82.35% agreement between predicted vulnerability classes and measured contamination levels [17]. In the Fasarood plain of southern Iran, Zarei et al. (2022) compared four vulnerability models, DRASTIC, fuzzy-based DRASTIC, composite DRASTIC, and a nitrate vulnerability index, across the same aquifer and found that all four indicated very low to moderate intrinsic vulnerability, but the composite DRASTIC produced the tightest spatial correlation with measured groundwater quality parameters [18]. Sensitivity analysis across both studies identified depth to water table and net recharge as the most influential parameters, together accounting for over 40% of the total vulnerability index weight.

In the Kherran plain of Khuzestan province, Iran, Chitsazan and Akhtari (2009) applied DRASTIC to an alluvial aquifer overlying a petroleum-producing region and confirmed that areas with shallow water tables (¡5 m), permeable sandy soils, and proximity to petroleum infrastructure received the highest vulnerability scores [19]. In the Hamadan–Bahar aquifer of western Iran, Jalali and Kolahchi (2019) compared DRASTIC, GOD, SINTACS, and the Susceptibility Index (SI) simultaneously and found that 7.1%, 29.56%, 44.21%, and 20.16% of the area, respectively, were classified as high vulnerability, a fourfold range in high-vulnerability area estimates from the same hydrogeological input data [20]. The GOD index, a simpler three-parameter model evaluating groundwater occurrence, overall lithology, and depth to water table, consistently produced more conservative vulnerability estimates than DRASTIC, reflecting its exclusion of recharge, soil media, and hydraulic conductivity from the scoring.

Modified DRASTIC variants have been developed to account for petroleum-specific contamination pathways. Umar et al. (2024) introduced a pipeline proximity parameter into the standard DRASTIC framework for the Ahoada communities of Nigeria's Niger Delta, where oil spills from pipeline interdiction are the dominant contamination source [21]. The modified model was validated against measured PAH concentrations in groundwater using ROC/AUC curves, and the pipeline-adjusted index outperformed conventional DRASTIC in predicting contamination hotspots [21]. In the Karak district of Khyber Pakhtunkhwa, Pakistan, Muneer et al. (2025) applied DRASTIC across a fold-and-thrust belt terrain and found that fractured zones with shallow water tables near petroleum exploration areas received vulnerability indices exceeding 150, classified as high- to very-high risk, while deeper confined aquifers beneath clay-rich formations scored below 100 [22].

Physically-based alternatives avoid the subjectivity of index weighting. Soriano et al. (2022) assessed shallow groundwater vulnerability to contamination from unconventional hydrocarbon extraction across a 104,000 km² region of Pennsylvania, Ohio, and West Virginia using a coupled MODFLOW-6/MODPATH-7 model at a 250 m grid resolution [23]. The model simulated contaminant travel times from surface spill locations to domestic well depths and identified zones where transport times fell below 18 years. Machine learning metamodels trained on the physically-based results achieved comparable predictions at a fraction of the computational cost, though spatial transferability between subdomains varied, models trained in one geological setting performed poorly when applied to dissimilar lithologies [23]. In British Columbia, Canada, Rosales-Ramirez et al. mapped DRASTIC parameters across 162,000 km² and fed the resulting parameter combinations into physically-based transport simulations, combining the spatial coverage of index methods with the process fidelity of numerical modeling [23].

3.3. Hydrogeological Controls on Contamination Severity

Depth to the water table outweighs all other parameters as a predictor of contamination severity. Zanello et al. (2021) simulated BTEX transport from residual fuel-phase contamination through sixty scenarios in Bahía Blanca, Argentina, combining three soil textures (silt loam, sandy loam, and clay), four water table depths (1.5, 2.5, 5, and 8 m), and three recharge rates [24]. In sandy loam, groundwater contamination risk was classified as very high for aquifers up to 8 m deep, regardless of recharge rate, while in silt loam and clay, risk dropped to moderate or low beyond 5 m of depth. When biodegradation was incorporated, leached concentrations fell by one to three orders of magnitude across all textures, but the relative ranking of depth as a control variable remained unchanged, biodegradation reduced absolute concentrations without altering the vulnerability hierarchy [24].

Lithology and hydraulic conductivity govern the velocity and geometry of contaminant migration. Karimova et al. (2021) modeled TPH transport through an alluvial aquifer beneath a petrochemical complex in the Pavlodar region of Kazakhstan, where transmissivity ranged from 22 to 133 m²/d and piezometric levels sat at 2–51 m below ground surface [25]. Particle tracking showed that contaminant plumes originating from monitoring wells near the refinery extended several kilometers downgradient within a decade, with transport velocities scaling directly with transmissivity. TPH concentrations in all monitoring wells exceeded the Kazakhstani permissible limit, confirming that the high-permeability alluvial sediments offered minimal retardation [25]. By contrast, clay-rich sequences act as effective barriers. The capillary zone experiments by Han et al. (2025) in fine sand and silty sand showed that LNAPL stopped flowing 20–40 cm above the water table in fine sand, a distance governed by moisture-dependent reductions in NAPL relative permeability, while coarse sand offered no comparable retardation [11].

Fracture networks in karst and crystalline aquifers create preferential pathways that bypass the matrix-based attenuation assumed by standard vulnerability models. Abo-Tabikh et al. (2025) documented heavy fuel oil contamination of a karst aquifer beneath the Al Hussein Thermal Power Station in northern Jordan, where groundwater velocities ranged from 218 m/day during base flow to 9,500 m/day during peak flow [26]. The contamination plume covered approximately 0.5 km² and was confined to the fractured Amman Formation chert limestone. Pump-and-treat remediation extracted 25,200 m^3 of contaminated water over three months, reducing TPH from over 10 mg/L to below 0.5 mg/L [26]. In southeastern Sicily, Ruggieri et al. (2017) recorded recharge velocities up to 230 m/h through the epikarst zone, orders of magnitude faster than transport through porous media, during an accidental drilling fluid loss at a petroleum exploration borehole that contaminated a public drinking water spring for weeks [27]. In Zibo City, Shandong Province, China, Guo et al. (2021) investigated a fractured karst aquifer contaminated by chlorinated hydrocarbons since the 1980s and found that the non-uniform hydrodynamic field created by high heterogeneity produced concentration oscillations of large amplitude over short time scales, detectable only through long-term continuous monitoring [28].

Water table fluctuation redistributes contamination vertically. The Sicilian industrial site tracked by Mineo and Ferrara (2022) showed that seasonal oscillations converted free-phase LNAPL to trapped residual during rising water levels and remobilized it during falling levels, producing apparent thickness variations in monitoring wells that correlated with oscillation amplitude [13]. This smear zone effect complicates remediation planning: apparent LNAPL thickness measured in wells overestimates the actual free-phase volume because trapped residual contributes to the observed thickness without being recoverable by skimming [13].

3.4. Assessment and Monitoring Methods

Hydrochemical monitoring at petroleum-contaminated sites relies on a combination of primary contaminant indicators (TPH, BTEX, PAH) and secondary redox parameters that track biodegradation status. Cozzarelli et al. (2022) analyzed four decades of groundwater chemistry downgradient of the 1979 Bemidji crude oil spill and documented a characteristic redox zonation: dissolved oxygen depleted within meters of the source, followed by sequential consumption of nitrate, ferric iron, and sulfate, with methanogenesis dominating the plume core [29]. Dissolved methane concentrations exceeded 14 mg/L in the most reduced zones, while benzene concentrations had declined by over 90% relative to peak values recorded in the 1990s, a trajectory attributable to sustained natural attenuation rather than active remediation [29]. Babika et al. (2024) sampled 15 stations along the Kporghor River sub-catchment in the Niger Delta and found groundwater TPH concentrations of 3–473 mg/L and total PAH concentrations up to 0.28 mg/L, with 54–100% of stations exceeding Nigerian and international water quality criteria [30].

Compound-specific isotope analysis (CSIA) provides a process-based line of evidence for biodegradation that concentration data alone cannot supply. Mancini et al. (2002) measured $\delta^{13}C$ and $\delta^{2}H$ in dissolved benzene and ethylbenzene downgradient of the source zone at the Dow Benelux industrial complex in the Netherlands [31]. Benzene $\delta^{13}C$ values were enriched by up to 2 ± 0.5 ‰ relative to the source, while $\delta^{2}H$ enrichments reached 27 ± 5 ‰ for benzene and 50 ± 5‰ for ethylbenzene, fractionation patterns consistent with anaerobic biodegradation and inconsistent with dilution or sorption, which produce no measurable isotopic shift [31]. Sherwood Lollar et al. (2022) applied dual-isotope CSIA across a mixed chlorobenzene-BTEX plume at a retired chemical manufacturing facility in New Jersey and estimated 47–99% degradation of 1,2-dichlorobenzene and 21–73% degradation of 1,2,4-trichlorobenzene using the Rayleigh equation, providing degradation quantification that concentration monitoring alone could not distinguish from dilution effects [32]. Li et al. (2024) tracked BTEX and chlorobenzene natural attenuation over five years (2016–2021) in a contaminated aquifer in Shandong, China, using both concentration trends and $\delta^{13}C$ enrichments ranging from +2.9 to +27.3 ‰, confirming that sulfate-reducing and fermenting bacteria were driving in situ degradation under anaerobic conditions [33].

Geophysical screening provides spatial characterization of contamination geometry that point-based chemical sampling cannot achieve. The companion review to this manuscript evaluates the diagnostic performance of electrical resistivity imaging, induced polarization, ground-penetrating radar, seismic, and integrated multi-method approaches for differentiating hydrocarbon from groundwater signatures at contaminated sites. That synthesis concluded that ERT-IP offers the most field-validated combination for plume delineation, while GPR adds thin-layer detection capability in low-conductivity vadose zone settings. Li et al. (2024) applied time-domain induced polarization imaging at a former chemical plant in eastern China and found that conductivity anomalies below 5 mS/m delineated the contaminated area consistent with borehole sampling data, while phase values below 20 mrad distinguished the LNAPL source zone from the dissolved plume, a discrimination that resistivity alone could not make [34].

Conceptual site models (CSMs) integrate geological, hydrogeological, and contamination data into a spatial framework that guides both risk assessment and remediation design. The ITRC (2018) LNAPL guidance established a tiered CSM approach: the LNAPL conceptual site model (LCSM) synthesizes information on source history, LNAPL distribution, migration potential, and natural attenuation status into a single interpretive framework that evolves as new data become available [35]. The Bemidji LCSM has been refined over four decades, incorporating subsurface temperature monitoring, soil gas profiling, and NSZD rate measurements to track the transition from an actively migrating plume to a stable, biodegradation-dominated system [14, 29].

4. Discussion

Aquifer properties shape contamination outcomes more than spill characteristics do. Zanello et al. (2021) showed that sandy loam aquifers stayed at very high risk when the water table sat within 16 m of the surface, regardless of how much rainfall pushed contaminants downward, while silt loam and clay dropped to moderate risk beyond 5 m from the same modeled source [24]. Once petroleum reaches the saturated zone, the host geology dictates the rest. At Pavlodar, high-transmissivity alluvium carried TPH plumes kilometers from the refinery within years [25]. In southeastern Sicily, epikarst recharge velocities of 230 m/h during a single drilling incident contaminated a public water spring within hours [27]. The two settings share little beyond the fact that petroleum entered the ground; everything about plume geometry, transport rate, and remediation difficulty followed from the aquifer, not the oil.

DRASTIC and its variants reduce this complexity to a single index score, convenient for regional screening but blind to how contamination changes after the initial release. Biodegradation, in particular, operates on timescales that static vulnerability maps ignore. The Bemidji record documents four decades of LNAPL mass loss driven overwhelmingly by gaseous-phase processes, methane and CO_2 outgassing, rather than the dissolved-phase attenuation that earlier mass-balance models assumed was dominant [15]. Across 40 LNAPL sites, Kulkarni et al. (2022) measured NSZD rates spanning two orders of magnitude, from 650 to 152,000 L/ha/yr [9], and the California dual-source study tied the dominant mechanism to LNAPL composition: methanogenesis for aliphatic-rich zones and vaporization for aromatic-rich zones [16]. A DRASTIC map drawn from borehole logs and soil surveys at the time of a spill cannot anticipate which pathway will dominate, how fast mass will be depleted, or when the plume will stabilize. Jalali and Kolahchi (2019) made this limitation concrete by running four index models on identical hydrogeological data in western Iran and getting high-vulnerability area estimates ranging from 7% to 44% of the study area [20]. When the model choice changes the answer more than the input data, the method has a credibility problem for site-level decisions.

Figure 2 compares the three assessment tiers and the escalation logic connecting them.

Process-based transport modeling avoids subjective weighting but trades it for data demands that few sites outside research basins can meet. The Appalachian Basin MODFLOW experiment by Soriano et al. (2022) showed that machine learning metamodels could approximate the full model at reduced cost, but only within the geological subdomain where they were trained. Applied to lithologically different areas,

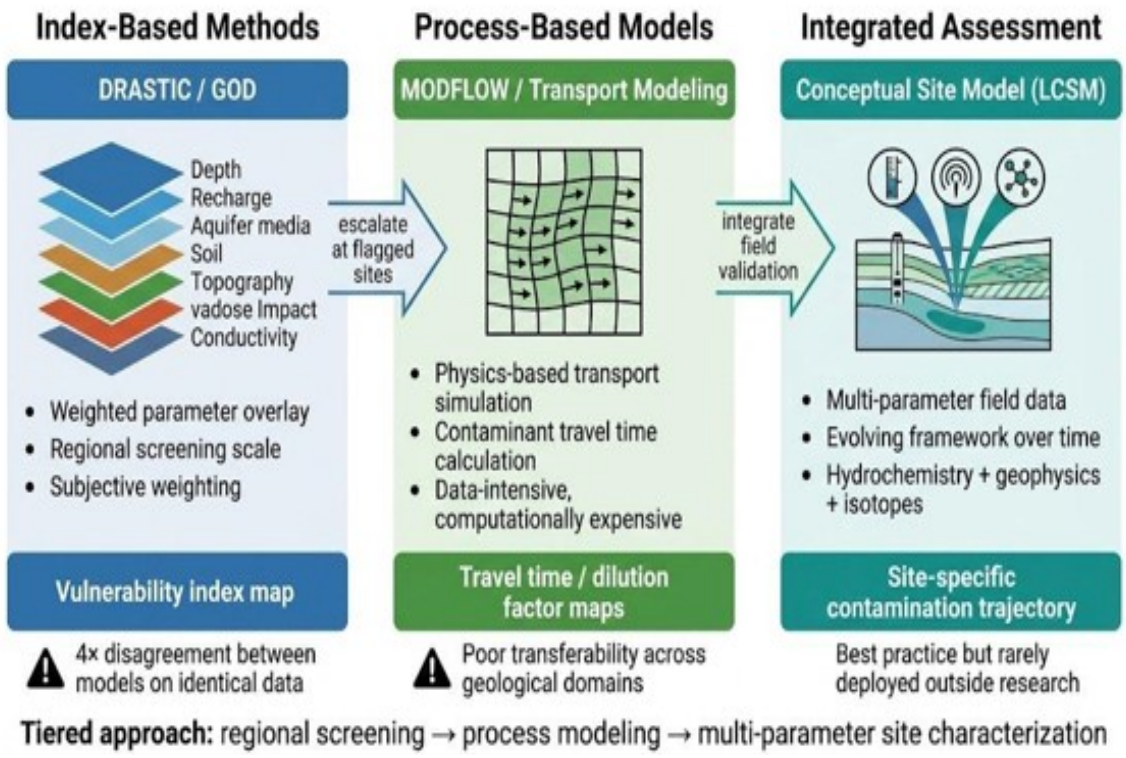

Figure 2: Comparison of three aquifer vulnerability assessment approaches

predictions degraded [23]. Coupling index screening with targeted process modeling at flagged sites is a sensible workflow, though it has been tested at only a handful of locations and no standardized protocol exists for deciding when to escalate from one tier to the next.

CSIA can quantify biodegradation extent, distinguish it from dilution, and identify reaction mechanisms, demonstrated at the Dow Benelux site, in New Jersey, and in Shandong [31–33]. Time-domain IP imaging can separate source zones from dissolved plumes where resistivity cannot [34]. Evolving conceptual site models built on multiparameter data, the LCSM framework gives the most accurate picture of contamination trajectory [35]. Most field investigations, though, still sample TPH and BTEX from a few wells once or twice a year, without redox profiling or spatial geophysics. Regulatory minimum requirements and cost pressures, not technical limits, account for the difference.

The geographic distribution of the evidence reviewed here is uneven. Detailed multi-parameter and long-term monitoring studies are concentrated in the United States, western Europe, and China. Major petroleum-producing regions, including the Middle East, Central Asia, West Africa, and Latin America, appear mainly through vulnerability mapping exercises with limited field validation. The NSZD and CSIA literature leans on a small set of research sites (Bemidji, the California dual-source site, Dow Benelux), and the attenuation rates and fractionation patterns measured there may not hold in aquifers with different mineralogy or microbial ecology. Prospective validation of vulnerability predictions, testing whether high-index zones actually contaminate faster or more severely than low-index zones after a subsequent release, is virtually nonexistent. English-language restriction likely excluded petroleum hydrogeology work published in Russian, Chinese, and Portuguese.

5. Conclusions

The aquifer matters more than the spill. Depth to the water table, lithology, fracture connectivity, and the geochemical conditions supporting biodegradation together determine whether a petroleum release becomes a localized nuisance or a regional groundwater crisis, and they do so regardless of whether the source is a wellsite, a pipeline, or a fuel station. DRASTIC and similar indices can rank relative vulnerability across a region, but applying four different index models to the same hydrogeological data produced vulnerability estimates that disagreed by a factor of four, which limits confidence in any single index score for site-level planning. Biodegradation adds a temporal dimension that no static index captures: NSZD rates spanning two orders of magnitude across 40 sites, and dominant attenuation mechanisms shifting with LNAPL composition, mean that vulnerability at the time of release may bear little resemblance to contamination status a decade later. The analytical tools needed to track these changes, isotope fractionation for biodegradation, induced polarization for source-plume separation, and evolving conceptual site models for long-term trajectory, are mature and field-proven but seldom deployed outside research settings. Regulatory assessment protocols built around periodic TPH sampling from a few wells cannot capture what these methods can. Tiered site characterization and index screening at the regional scale, followed by a multiparameter investigation where the screening flags concern, would bring standard practice closer to what the science already supports.

Article Information

Acknowledgements: The authors acknowledge the contributions of researchers whose work was included in this review and the institutions that supported access to scientific databases.

Author Contributions: Bernard Nkrumah Attobrah - Conceptualization, Literature search and data curation, Methodology, Writing – original draft preparation, Writing – review and editing; Emmanuel Kobina Gyasi - Conceptualization, Literature search and data curation, Writing – review and editing; Aderemi Sarah Aduloju - Conceptualization, Supervision, Writing – review and editing; Elijah Asamoah Amoateng - Literature search and data curation, Writing – review and editing; Enoch Nii-Okai - Literature search and data curation, Writing – review and editing; Jonathan Kuffour Owusu - Methodology, Writing – review and editing; Mariam Iyabo Adeoba - Methodology, Writing – review and editing.

Funding: The authors declare that no specific funding was received for this work from any funding agency in the public, commercial, or not-for-profit sectors.

Competing Interests: The authors declare that they have no competing financial or non-financial interests.

Ethical Approval: Not applicable. This study is a narrative review based on previously published data and does not involve human participants, animals, or primary data collection.
Consent to Participate: Not applicable.

Consent for Publication: Not applicable.

Data Availability: No new datasets were generated or analyzed in this study. All data supporting the findings are derived from previously published studies cited in the manuscript.

Use of Artificial Intelligence: The authors declare that generative artificial intelligence tools (e.g., language models) were used only for language refinement and editing support. All scientific content, interpretation, and conclusions were developed independently by the authors, who take full responsibility for the integrity of the work.

References

[1] P. Li and J. Wu. Sources and consequences of groundwater contamination. *Archives of Environmental Contamination and Toxicology*, 80:1–10, 2021.

[2] U. Lall, L. Josset, and T. Russ. A snapshot of the world's groundwater challenges. *Annual Review of Environment and Resources*, 45: 171–194, 2020.

[3] S. Kuppusamy, N. R. Maddela, M. Megharaj, and K. Venkateswarlu. *Total Petroleum Hydrocarbons: Environmental Fate, Toxicity, and Remediation*. Springer, 2020.

[4] B. Fei-Baffoe et al. Contamination of groundwater by petroleum hydrocarbons: impact of fuel stations in residential areas. *Heliyon*, 10 (3):e25433, 2024.

[5] S. Kuppusamy et al. Petroleum hydrocarbons (PH) in groundwater aquifers: an overview of environmental fate, toxicity, microbial degradation and risk-based remediation approaches. *Frontiers of Environmental Science Engineering*, 11:26, 2017.

[6] S. Mineo. Groundwater and soil contamination by LNAPL: state of the art and future challenges. *Science of the Total Environment*, 874:162394, 2023.

[7] E. A. Atekwana and E. A. Atekwana. Geophysical signatures of microbial activity at hydrocarbon contaminated sites: a review. *Surveys in Geophysics*, 31:247–283, 2010.

[8] A. Barbulescu. Assessing groundwater vulnerability: DRASTIC and DRASTIC-like methods: a review. *Water*, 12(5):1356, 2020.

[9] P. R. Kulkarni, K. L. Walker, C. J. Newell, K. K. Askarani, Y. Li, and T. E. McHugh. Natural source zone depletion (NSZD) insights from over 15 years of research and measurements: a multi-site study. *Water Research*, 225:119170, 2022.

[10] R. Zuo, X. Zhao, J. Yang, M. Pan, Z. Xue, X. Gao, J. Wang, and Y. Teng. Analysis of the LNAPL migration process in the vadose zone under two different media conditions. *International Journal of Environmental Research and Public Health*, 18(21):11073, 2021. URL https://doi.org/10.3390/ijerph182111073.

[11] D. Han et al. Effect and mechanism of the moisture content on the kinetic retardation of LNAPL pollutant migration by the capillary zone. *Journal of Hazardous Materials*, 2025. URL https://doi.org/10.1016/j.jhazmat.2025.137297.

[12] K. Suo, M. Zhao, Y. Liu, H. Liu, and M. Jia. A study on the monitoring of LNAPL migration using ERT. *PLoS ONE*, 20(1):e0315624, 2025. URL https://doi.org/10.1371/journal.pone.0315624.

[13] S. Mineo and A. Ferrara. Evolution of LNAPL contamination plume in fractured aquifers. *Bulletin of Engineering Geology and the Environment*, 81:296, 2022. URL https://doi.org/10.1007/s10064-022-02627-w.

[14] H. I. Essaid, B. A. Bekins, W. N. Herkelrath, and G. N. Delin. Crude oil at the Bemidji site: 25 years of monitoring, modeling and understanding. *Groundwater*, 49:706–726, 2011.

[15] G.-H. C. Ng, B. A. Bekins, I. M. Cozzarelli, M. J. Baedecker, P. C. Bennett, and R. T. Amos. Reactive transport modeling of geochemical controls on secondary water quality impacts at a crude oil spill site near Bemidji, MN. *Water Resources Research*, 51: 4156–4183, 2015.

[16] D. M. Mackay et al. Impacts of LNAPL types on mechanisms and rate of natural source zone depletion. *Environmental Pollution*, 355: 124210, 2024.

[17] M. K. Jha et al. Assessment of groundwater pollution vulnerability using GIS-based DRASTIC model and its validation using nitrate concentration in Tandula watershed, Chhattisgarh, India. *Journal of the Geological Society of India*, 93:567–573, 2019.

[18] A. R. Zarei et al. Assessment of groundwater vulnerability using GIS-based modified DRASTIC models, case study: Fasarood Plain, South Iran. *Journal of Environmental Assessment Policy and Management*, 24(4), 2022.

[19] M. Chitsazan and Y. Akhtari. A GIS-based DRASTIC model for assessing aquifer vulnerability in Kherran Plain, Khuzestan, Iran. *Water Resources Management*, 23:1137–1155, 2009.

[20] M. Jalali and Z. Kolahchi. Groundwater vulnerability assessment with using GIS in Hamadan–Bahar plain, Iran. *Applied Water Science*, 9:196, 2019.

[21] H. A. Umar et al. Application of modified DRASTIC model for oil spills pollution affecting water quality system in part of Niger Delta region of Nigeria. *Journal of Hydrology*, 637:131354, 2024.

[22] M. Muneer et al. Assessment of groundwater intrinsic vulnerability using GIS-based DRASTIC method in district Karak, Khyber Pakhtunkhwa, Pakistan. *Frontiers in Water*, 7, 2025. Article 1540703.

[23] M. A. Soriano et al. Regional scale assessment of shallow groundwater vulnerability to contamination from unconventional hydrocarbon extraction. *Environmental Science Technology*, 56:12126–12136, 2022.

[24] V. Zanello et al. Assessment of groundwater contamination risk by BTEX from residual fuel soil phase. *Discover Applied Sciences*, 3: 364, 2021.

[25] B. Karimova et al. Assessing data-scarce contaminated groundwater sites surrounding petrochemical industries. *Environmental Earth Sciences*, 80:354, 2021.

[26] M. Abo-Tabikh et al. Groundwater remediation action plan of polluted aquifer by heavy fuel oil, Northern Jordan. *Water Supply*, 25(2): 343–358, 2025.

[27] G. Ruggieri et al. Accidental contamination during hydrocarbon exploitation and the rapid transfer of heavy-mineral fines through an overlying highly karstified aquifer. *Journal of Hydrology*, 546:269–282, 2017.

[28] Y. Guo et al. Contamination characteristics of chlorinated hydrocarbons in a fractured karst aquifer using TMVOC and hydro-chemical techniques. *Science of the Total Environment*, 790:148030, 2021.

[29] I. M. Cozzarelli, M. J. Baedecker, A. C. Mumford, J. B. Jaeschke, and T. A. Spencer. Understanding the evolution of groundwater-contaminant plume chemistry emanating from legacy contaminant sources. *Groundwater Monitoring Remediation*, 42:30–42, 2022.

[30] Z. M. Babika et al. Assessing petroleum contamination in parts of the Niger Delta based on a sub-catchment delineated field assessment. *Environmental Monitoring and Assessment*, 196:561, 2024.

[31] S. A. Mancini et al. Hydrogen isotopic enrichment: an indicator of biodegradation at a petroleum hydrocarbon contaminated field site. *Environmental Science Technology*, 36:2464–2470, 2002.

[32] B. Sherwood Lollar et al. Compound-specific isotope analysis (CSIA) evaluation of degradation of chlorinated benzenes and benzene in a contaminated aquifer. *Journal of Contaminant Hydrology*, 248:104014, 2022.

[33] S. Li et al. Natural attenuation of BTEX and chlorobenzenes in a formerly contaminated pesticide site in China: Examining kinetics, mechanisms, and isotopes analysis. *Science of the Total Environment*, 912:169230, 2024.

[34] Y. Dong, T. Xia, J. Meng, and D. Mao. Imaging LNAPL distribution at a former chemical plant with time-domain induced polarization. *Scientific Reports*, 14:18268, 2024. doi: 10.1038/s41598-024-66782-8.

[35] ITRC. *LNAPL Site Management: LCSM Evolution, Decision Process and Remedial Technologies. LNAPL-3*. Interstate Technology Regulatory Council, 2018.